Defense Threat Reduction Agency
8725 John J. Kingman Road, MS
6201 Fort Belvoir, VA 22060-6201

DTRA-TR-13-23

TECHNICAL REPORT

Synthesis, Characterization, and Multimillion-Atom Simulation of Halogen-Based Energetic Materials for Agent Defeat

Approved for public release; distribution is unlimited.

April 2013

HDTRA1-08-1-0036

Karl O. Christe, et al.

Prepared by:
University of Southern California
Los Angeles, CA 33777

DESTRUCTION NOTICE:

Destroy this report when it is no longer needed.
Do not return to sender.

PLEASE NOTIFY THE DEFENSE THREAT REDUCTION AGENCY, ATTN: DTRIAC/ J-3 ONIUI , 8725 JOHN J. KINGMAN ROAD, MS-6201, FT BELVOIR, VA 22060-6201, IF YOUR ADDRESS IS INCORRECT, IF YOU WISH THAT IT BE DELETED FROM THE DISTRIBUTION LIST, OR IF THE ADDRESSEE IS NO LONGER EMPLOYED BY YOUR ORGANIZATION.

REPORT DOCUMENTATION PAGE

Form Approved
OMB No. 0704-0188

1. REPORT DATE *(DD-MM-YYYY)*	**2. REPORT TYPE**	**3. DATES COVERED** *(From - To)*
00-04-2013	Technical	April 23, 2008 – June 22, 2012

4. TITLE AND SUBTITLE

Synthesis, Characterization, and Multimillion-Atom Simulation of Halogen-based Energetic Materials for Agent Defeat

5a. CONTRACT NUMBER
HDTRA1-08-1-0036

5b. GRANT NUMBER

5c. PROGRAM ELEMENT NUMBER

6. AUTHOR(S)

Karl O. Christe, Ralf Haiges, and Priya Vashista

5d. PROJECT NUMBER

5e. TASK NUMBER

5f. WORK UNIT NUMBER

7. PERFORMING ORGANIZATION NAME(S) AND ADDRESS(ES)

Loker Research Institute and Dept of Chemistry,
and Dept for Computer Science,
University of Southern California, Los Angeles, CA 90089

8. PERFORMING ORGANIZATION REPORT NUMBER

USC-DTRA-F-2012

9. SPONSORING / MONITORING AGENCY NAME(S) AND ADDRESS(ES)

Defense Threat Reduction Agency
8725 John J. Kingman Road STOP 6201
Fort Belvoir, VA 22060
PM/S. Peiris

10. SPONSOR/MONITOR'S ACRONYM(S)

DTRA

11. SPONSOR/MONITOR'S REPORT NUMBER(S)

DTRA-TR-13-23

12. DISTRIBUTION / AVAILABILITY STATEMENT

Approved for public release; distribution is unlimited.

13. SUPPLEMENTARY NOTES

14. ABSTRACT

The previously unknown I2O7 was successfully synthesized and characterized. The only missing piece of information is a crystal structure. It was shown that it is of insufficient thermal stability, but that the known I2O6 is an excellent substitute. The literature synthesis for I2O6 was drastically improved and scaled up to the 100 g level. Several hundred gram of I2O6 were prepared and provided to Prof. Vashistha (USC), Prof. Dreizin (NJ Inst. of Technology), Prof. Zachariah (U of Maryland), Dr. Higa (NAVAIR, China Lake), Dr. Lightstone (Indian Head), Dr. Liu (NIST) and Dr. Kolesnikov (Oakridge) for further evaluation. Explosives testing at NAVAIR and Indian Head, powder diffraction measurements at NIST and neutron diffraction and inelastic scattering experiments at Oakridge have been highly successful. At the suggestion of Dr. Su Peiris, coating studies for I2O6 were also carried out which resulted in an improvement of its hydrolytic stability.
First-principle quantum-mechanical calculations of I2O5 and I2O6 crystals were carried out to investigate their structural and lattice-dynamic properties. Their equations of states and thermodynamic properties at high pressures and temperatures were also calculated.

15. SUBJECT TERMS

Iodine oxides, iodine heptoxide, iodine hexoxide, agent defeat

16. SECURITY CLASSIFICATION OF:			**17. LIMITATION OF ABSTRACT**	**18. NUMBER OF PAGES**	**19a. NAME OF RESPONSIBLE PERSON**
a. REPORT	**b. ABSTRACT**	**c. THIS PAGE**	SAR	38	Suhithi Peiris
Unclassified	Unclassified	Unclassified			**19b. TELEPHONE NUMBER** *(include area code)* 703-767-4732

CONVERSION TABLE

Conversion Factors for U.S. Customary to metric (SI) units of measurement.

MULTIPLY →	BY →	TO GET
TO GET ←	BY ←	DIVIDE
angstrom	1.000 000 x E -10	meters (m)
atmosphere (normal)	1.013 25 x E +2	kilo pascal (kPa)
bar	1.000 000 x E +2	kilo pascal (kPa)
barn	1.000 000 x E -28	meter^2 (m^2)
British thermal unit (thermochemical)	1.054 350 x E +3	joule (J)
calorie (thermochemical)	4.184 000	joule (J)
cal (thermochemical/cm^2)	4.184 000 x E -2	mega joule/m^2 (MJ/m^2)
curie	3.700 000 x E +1	*giga bacquerel (GBq)
degree (angle)	1.745 329 x E -2	radian (rad)
degree Fahrenheit	$t_k = (t^\circ f + 459.67)/1.8$	degree kelvin (K)
electron volt	1.602 19 x E -19	joule (J)
erg	1.000 000 x E -7	joule (J)
erg/second	1.000 000 x E -7	watt (W)
foot	3.048 000 x E -1	meter (m)
foot-pound-force	1.355 818	joule (J)
gallon (U.S. liquid)	3.785 412 x E -3	meter^3 (m^3)
inch	2.540 000 x E -2	meter (m)
jerk	1.000 000 x E +9	joule (J)
joule/kilogram (J/kg) radiation dose absorbed	1.000 000	Gray (Gy)
kilotons	4.183	terajoules
kip (1000 lbf)	4.448 222 x E +3	newton (N)
kip/$inch^2$ (ksi)	6.894 757 x E +3	kilo pascal (kPa)
ktap	1.000 000 x E +2	newton-second/m^2 ($N-s/m^2$)
micron	1.000 000 x E -6	meter (m)
mil	2.540 000 x E -5	meter (m)
mile (international)	1.609 344 x E +3	meter (m)
ounce	2.834 952 x E -2	kilogram (kg)
pound-force (lbs avoirdupois)	4.448 222	newton (N)
pound-force inch	1.129 848 x E -1	newton-meter (N-m)
pound-force/inch	1.751 268 x E +2	newton/meter (N/m)
pound-force/$foot^2$	4.788 026 x E -2	kilo pascal (kPa)
pound-force/$inch^2$ (psi)	6.894 757	kilo pascal (kPa)
pound-mass (lbm avoirdupois)	4.535 924 x E -1	kilogram (kg)
pound-mass-$foot^2$ (moment of inertia)	4.214 011 x E -2	kilogram-meter^2 ($kg-m^2$)
pound-mass/$foot^3$	1.601 846 x E +1	kilogram-meter^3 (kg/m^3)
rad (radiation dose absorbed)	1.000 000 x E -2	**Gray (Gy)
roentgen	2.579 760 x E -4	coulomb/kilogram (C/kg)
shake	1.000 000 x E -8	second (s)
slug	1.459 390 x E +1	kilogram (kg)
torr (mm Hg, 0^0 C)	1.333 22 x E -1	kilo pascal (kPa)

*The bacquerel (Bq) is the SI unit of radioactivity; 1 Bq = 1 event/s.

**The Gray (GY) is the SI unit of absorbed radiation.

Table of Contents

Foreword

The first three years (04/23/2008 – 06/22/2011) of this program involved the joint efforts of two groups, the synthesis group with Prof. Karl Christe as PI and the simulation group with Prof. Priya Vashista as the PI. On June 22, 2011, DTRA granted a two year extension to the synthesis effort by the Christe group, and awarded Dr. Ken-ichi Nomura a 2-year Young Investigator Award to continue the exploration of the computational part of the project. This report summarizes the results obtained by both groups during the original program and the results obtained by the Christe group under the synthesis extension program.

Objectives

Chemical and biological agents (CBAs) represent a serious threat to our homeland security. Once these agents become airborne over large areas, they become very difficult to destroy. Consequently, it is desirable to either destroy these agents before they can escape from their storage or production facilities or, even better, to destroy them simultaneously with the entire facility. One can envision a combined weapon system in which tailored explosives would destroy the storage or production facility, while secondary chemical reagents would neutralize the CBAs. Therefore, the objectives of this proposal were the development of powerful novel chemical reagents for the destruction of biologically active materials and a simulation of their reactions on a multimillion atom scale with quantum mechanical accuracy to study the stability of the reactive species under high-temperature and high-pressure fireball conditions.

More specifically, we have been synthesizing and characterizing novel halogen oxidizers for formulation with high-performance explosives (HMX or RDX) to produce over-oxidized explosives for destruction of chemical & biological agents. Multimillion-atom molecular dynamics simulations with quantum mechanical accuracy were used to study the stability of the halogen species in high-temperature and high-pressure fireballs. Ideal candidates for these over-oxidized explosives were mixtures of HMX or RDX with halogen

oxides in their highest oxidation states. Of these halogen oxides, the unknown I_2O_7 originally was our preferred choice. It was predicted to be thermally stable and insensitive and to possess a density in excess of 4.5 g/cm^3. Therefore, the premier goal of our proposed study was the synthesis and characterization of this compound. However, other sources for positive halogen compounds, such as molecular I_2O_6, IO_3F, IF_5O, and IF_3O_2, IF_3O, ionic IF_4O^+, IO_3^+, IF_6O^-, IF_4O^-, $IF_4O_2^-$, $IF_5O_2^{2-}$, IF_5O^{2-} and $IF_6^+IO_4^-$ were also good target compounds.

The original program plan included the following milestones.

Year 1: Synthesis and characterization of I_2O_7 precursors, theoretical prediction of properties of I_2O_7 and modeling of iodine oxide/HMX using the known compounds I_2O_5 and I_2O_6.

Year 2: Synthesis and characterization of I_2O_6 and modeling of the I_2O_7 and I_2O_6 systems.

Year 3: Development of Scale-up synthesis and formulation testing of I_2O_6 and modeling of the complete system including CBAs.

The goals of the 2-year Synthesis Extension were: Preparation of larger amounts of I_2O_6 and their distribution to other laboratories for advanced formulation studies and testing; crystal structure determination of I_2O_7; and the development of coating techniques for I_2O_6 to improve its hydrolytic stability.

Summary of Efforts

Synthesis Task

Excellent progress was made during this program. We have successfully synthesized the previously unknown I_2O_7 and have characterized it. The only missing piece of information is a crystal structure. We have shown that it is of insufficient thermal stability, but that the known I_2O_6 is an excellent substitute. We have drastically improved the literature synthesis for I_2O_6, have scaled up its production to the 100 g level, have prepared several hundred gram of I_2O_6, and have provided Prof. Vashistha (USC), Prof. Dreizin (NJ Inst. of Technology), Prof. Zachariah (U of Maryland), Dr. Higa (NAVAIR,

China Lake), Dr. Lightstone (Indian Head), Dr. Liu (NIST) and Dr. Kolesnikov (Oakridge) with samples for further evaluation. Explosives testing at NAVAIR and Indian Head, powder diffraction measurements at NIST and neutron diffraction and inelastic scattering experiments at Oakridge have been highly successful. At the suggestion of Dr. Su Peiris, we have also carried out coating studies for I_2O_6 which resulted in an improvement of its hydrolytic stability.

Simulation Task

We have performed first-principle quantum-mechanical calculations of I_2O_5 and I_2O_6 crystals to investigate their structural and lattice-dynamic properties. We have also calculated their equations of states and thermodynamic properties at high pressures and temperatures. The results were summarized in a manuscript entitled: "Phonon Density of States of Iodine Oxides – I_2O_5 and I_2O_6: A Joint Study Using Neutron Scattering and First-principles Calculations," which will be submitted to Chem. Phys. Letters for publication.

Accomplishments/New Findings

Synthesis Task

The synthesis of the previously unknown I_2O_7 was achieved by the low-temperature dehydration of H_5IO_6 with SO_3 (eq.1).

$$2\ H_5IO_6\ +\ 5\ SO_3 \xrightarrow{H_2SO_4} I_2O_7\ +\ 5\ H_2SO_4 \qquad (1)$$

The I_2O_7 was identified by the observed material balance and its Raman spectrum which differs significantly from that of I_2O_6 (see Fig. 1). The observed Raman spectrum of I_2O_7 was also compared to that for the free I_2O_7 molecule calculated for us at the B3LYP/DZVP level by Prof. David Dixon at the University of Alabama. The comparison shows that the observed spectrum is much more complex than that calculated for the free gaseous molecule, and that I_2O_7 must possess an oxygen-bridged polymeric structure.

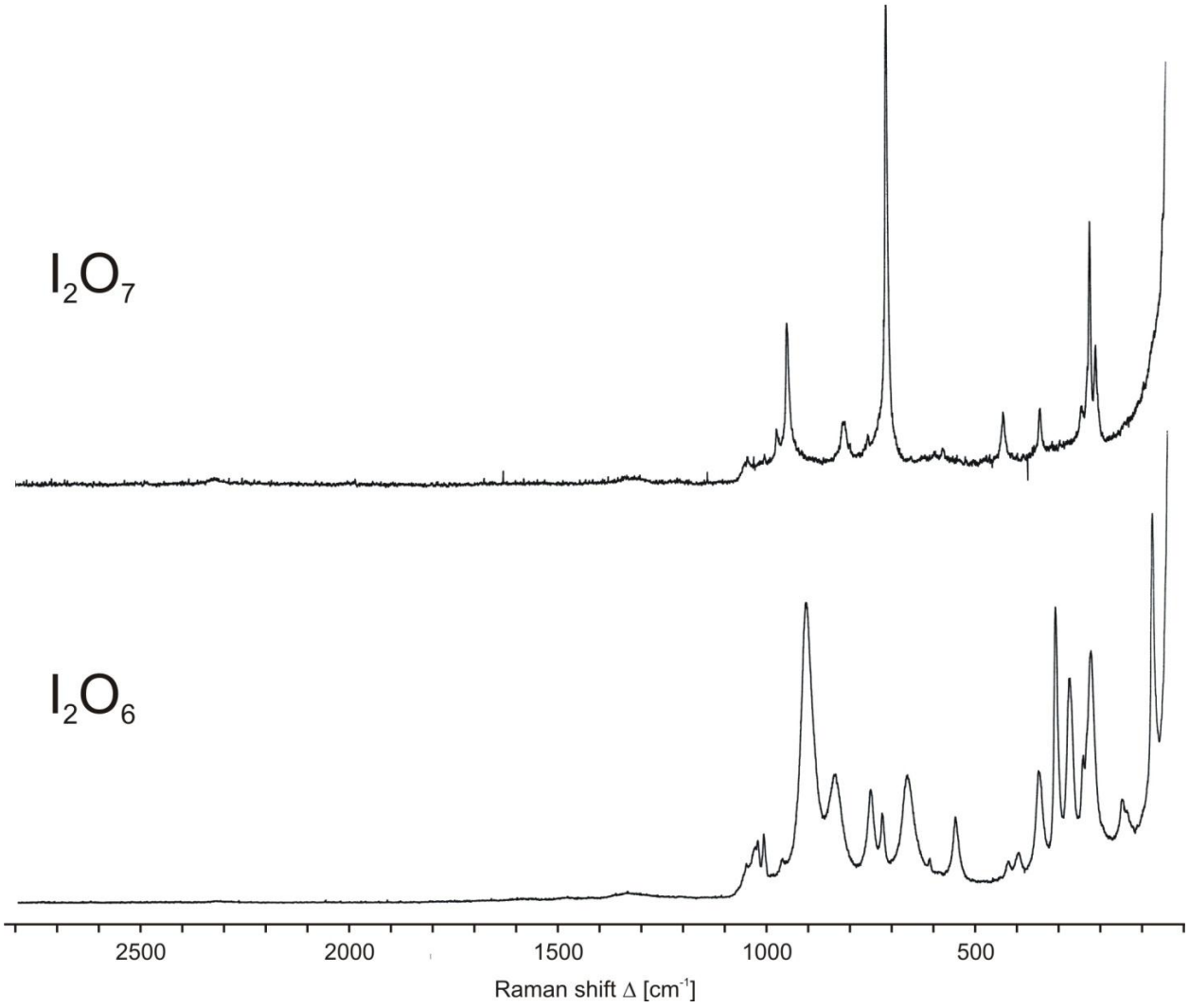

Figure 1. Raman spectra of I_2O_7 and I_2O_6

Therefore, a crystal structure is needed to establish the exact structure of solid I_2O_7. Efforts to grow single crystals of I_2O_7 were made but were impeded by its low solubility in all the tested solvents. The I_2O_7 is a marginally stable yellow solid which starts to lose dioxygen at room temperature and decomposes rapidly at 60 °C to give I_2O_6 (eq. 2).

$$2\ I_2O_7 \longrightarrow 2\ I_2O_6 + O_2 \qquad (2)$$

Because of its low thermal stability, I_2O_7 is not a good candidate for practical applications. However, our Thermo Gravimetric Analysis (TGA) and Differential Scanning Calorimetry (DSC) studies of I_2O_6 showed that this compound is thermally stable to about 187 °C, where it decomposes quantitatively to I_2O_5 and dioxygen (eq. 3).

$$2\ I_2O_6 \longrightarrow 2\ I_2O_5 + O_2 \qquad (3)$$

At about 400 °C, the I_2O_5 then decomposes to iodine and oxygen. A special differential scanning calorimeter was built (see Fig. 2) and used to measure (see Fig. 3) the heat of formation of I_2O_6. The DSC curve showed an exotherm with an onset of 179 ºC and a peak of 197 ºC for the decomposition of I_2O_6 to I_2O_5 and dioxygen, and an endotherm with an onset of 393 ºC and a peak of 424 ºC for the decomposition of I_2O_5 to the elements. From these data, the heat of formation of I_2O_6 was found to be -90.2 kJ/mol.

Figure 2. Differential Scanning Calorimeter

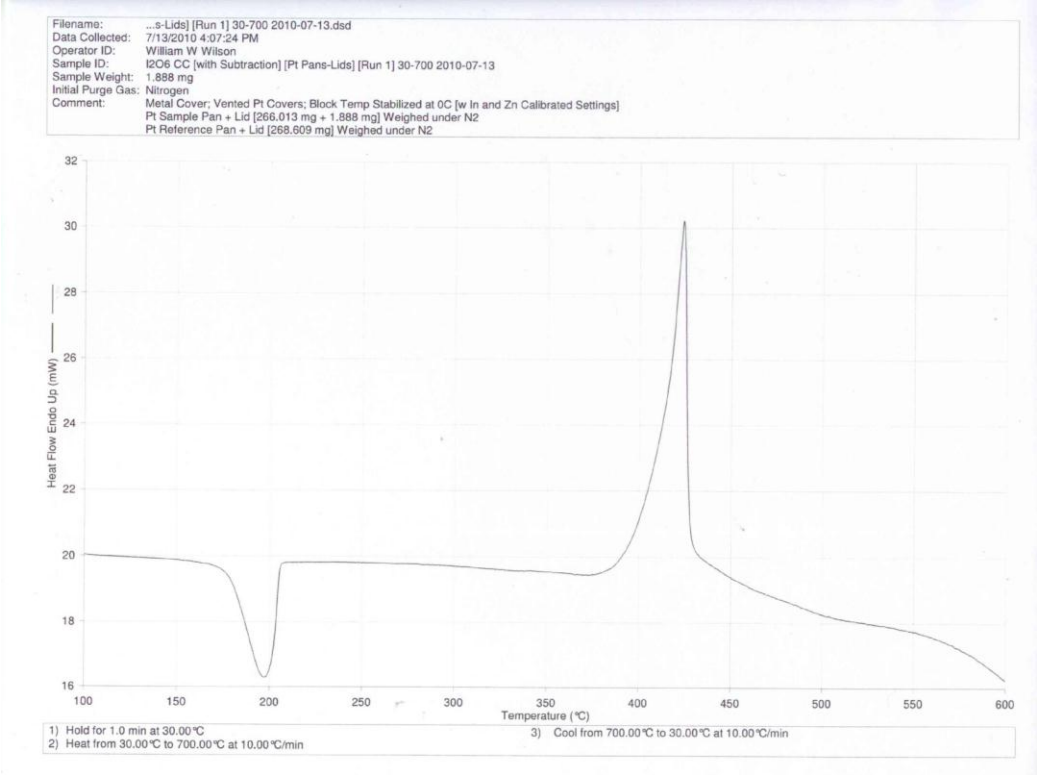

Figure 3. DSC Curve of I_2O_6

This heat of formation, combined with its density of 5.40 g/cm^3 (T. Kraft and M. Jansen, *J. Am. Chem. Soc.*, **1995**, *117*, 6795) and its ability to generate spore killing positive halogen compounds, makes I_2O_6 an outstanding candidate for the DTRA applications.

The crystal structure of I_2O_6 is well known (T. Kraft and M. Jansen, *J. Am. Chem. Soc.*, **1995**, *117*, 6795), but the published synthesis from H_5IO_6 and conc. H_2SO_4 had been very time consuming. We have, therefore, worked on an improved synthesis of I_2O_6. Instead of going through the decomposition of an intermediate I_2O_7, we have used equimolar amounts of iodic and periodic acids instead. In this way, we have shortened the reaction time from the previous one month to one day. We have scaled up the reaction to a 100 g level and have prepared several hundred g of I_2O_6. We have provided Prof. Vashistha (USC) with large samples for the neutron diffraction studies. We have also sent samples of I_2O_6 to Prof. Dreizin (NJ Inst. of Technology), Prof. Zachariah (U of Maryland), Dr. Higa (NAVAIR, China Lake), Dr. Lightstone (Indian Head), Dr. Liu (NIST) and Dr. Kolesnikov (Oakridge) with samples for further evaluation. We have also prepared a

sample of hydrogen-free I_2O_5 by pyrolysis of I_2O_6 for a neutron diffraction study by Dr. Kolesnikov at Oak Ridge.

Dr. Higa at NAVAIR has obtained very interesting results. While neat I_2O_6 reacted only slowly with 80 nm Al powder, the same mixture with an Al/MoO_3 bootstrap gave deflection rates about twice as large as those of an Al(320 nm)/Bi_2O_3 standard. Furthermore, the Al/I_2O_6 composite was stable on storage for more than 10 months. Very importantly, in all of these tests, the formation of elemental iodine was visually observed. Similar tests with I_2O_5 in place of I_2O_6 resulted only in half of the deflection rates and demonstrate that I_2O_6 is clearly superior to I_2O_5. A patent disclosure on these I_2O_6 based explosives has been submitted by Dr. Higa through NAVAIR.

Spore killing tests with Al/I_2O_6 formulations were carried out at NSWC Indian Head by Jillian Horne and Dr. Jim Lightstone. They found that the I_2O_6 formulations resulted in greatly improved temperature/time plots both in the detonation chamber and the exhaust chamber. Due to the unexpectedly high pressures obtained in these tests, the filters were blown out and they did not obtain data on the spore killing efficiency of these formulations. The tests must be repeated.

Since I_2O_6 is somewhat hygroscopic, Dr. Su Peiris suggested carrying out coating studies to improve its hydrolytic stability. In preliminary experiments, it was attempted to coat I_2O_6 with perfluorodecanoic, perfluorododecanoic and perfluorooctadecanoic (perfluorostearic) acid. For the experiments, samples of about 1 g of finely powdered I_2O_6 was stirred in about 10 mL of 10 weight % solutions of the perfluorinated acid in trifluoroacetic acid. The trifluoroacetic acid was then evaporated in a vacuum so that the dissolved perfluorinated acid resulted in a coating of the I_2O_6 particles. The obtained yellow powders were inspected by Raman spectroscopy. In all three cases, the characteristic bands of I_2O_6 together with the much weaker bands of the perfluorinated acid were present in the spectrum. The I_2O_6 samples were then exposed to the air and their decomposition followed by Raman spectroscopy. In all three cases the samples were less air sensitive than a sample of untreated I_2O_6. However, after an air exposure of about 4 hours, Raman bands characteristic for I_2O_5, HIO_3 and H_5IO_6 started to appear. This is clearly an indication that it is possible to make I_2O_6 more resistant to atmospheric moisture by coating it with perfluorinated compounds; however, more experimental work

in this area is needed. Future experiments would involve the use of perfluorinated or partially fluorinated alkohols such as ultrahigh molecular weight 2-(perfluoroalkyl)ethanol, perfluorododecan-1-ol, perfluorotetradecan-1-ol and perfluorohexadecan-1-ol as well as solutions of amorphous fluoropolymer (Teflon AF, "liquid Teflon").

Simulation Task

I. Structural Properties

The I_2O_5 crystal has the monoclinic structure and space group $P2_1/c$ with four molecules in the unit cell (see Fig. 4), whereas the I_2O_6 crystal has the triclinic structure and belongs to space group $P\bar{1}$ (see Fig. 5).

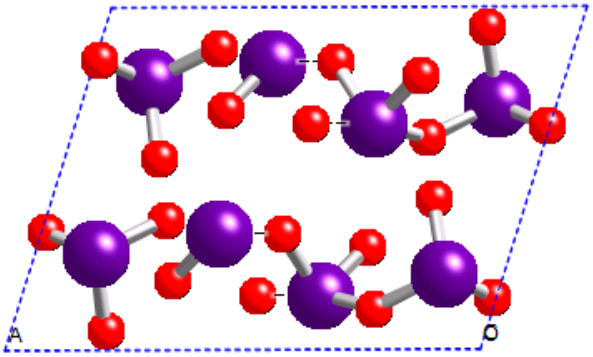

Figure 4. Crystal structure of I_2O_5.

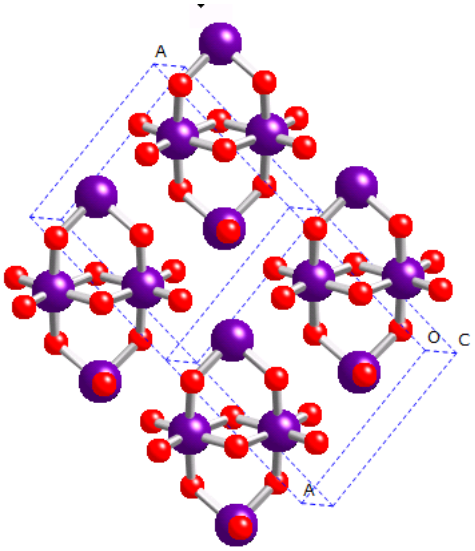

Figure 5. Crystal structure of I_2O_6.

The volumes calculated by DFT without van der Waals (VDW) correction are far larger than the experimental equilibrium volumes for the two iodine oxide crystals. Namely, the volume difference is 9.9% and 11.7% for I_2O_5 and I_2O_6, respectively. Such discrepancy is common in molecular crystals and has been ascribed to the inadequacy of exchange correlation functional in dealing with VDW interaction. After including the VDW correction, the calculated volume agrees well with the experiment data.

Calculation without VDW correction usually overestimates the bond lengths about 2-3%. In some bonds, the overestimation can be as large as 5%. Although VDW correction definitely decreases the volume, its effect on the bond length is not trivial. In I_2O_5, VDW correction in fact increases the bond lengths slightly except for one bond. The change of bond length caused by VDW correction is usually smaller than 1%. For I_2O_6, the effect of VDW on bond lengths depends on specific iodine atoms. The bonds from one I atom increase lengths, whereas bonds from another I atom decrease lengths by VDW correction. However, the change of the bond length is usually small.

For intermolecular distances, VDW correction always decreases them. In general, VDW correction makes these interatomic distances more consistent with the experimental value.

The effect of pressure on bond lengths is found to be similar to that of VDW correction. If the bond length increases/decreases with VDW correction, it increases/decreases with pressure. Specifically, all the bond length of I_2O_5 but one increases with the pressure. For I_2O_6, the bonds from one I atom increase the length and bonds from another I atom decrease the length with the pressure. Therefore, to some extent, the effect of the VDW correction can be viewed as the pressure effect.

II. Vibrational Properties

The phonon density of states (DOS) of I_2O_5 (Fig. 6) has a small gap located between 425 and 439 cm^{-1}. The detailed analysis of the vibrational modes (Fig. 7) indicates that the stretching modes and bending modes are separated by this gap. Above this gap, all the vibrational modes are stretching modes. There is another gap at a frequency of about 700 cm^{-1}, where the phonon DOS of I_2O_5 is considerably smaller than the rest. Above this frequency are the terminal I=O stretching modes and below it are the bridging I-O-I stretching modes. The frequencies of the stretching modes are sensitive to the bond

lengths. The calculation overestimates the bond lengths. This leads to an overall underestimation of the frequencies of the stretching modes. In contrast, the calculated frequencies agree well with the experimentally observed ones for the bending and the lattice modes.

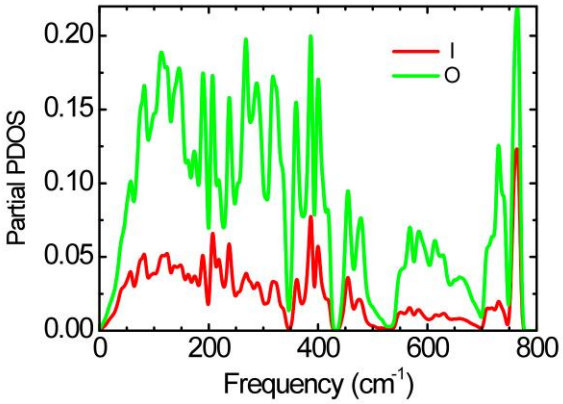

Figure 6. Partial phonon density of states of I_2O_5.

The Grüneisen parameter, which is defined as $\gamma_i = -d\ln\omega_i / d\ln V$, describes the volume dependence of the frequency. Since the bond lengths can increase slightly with the pressure, some of the stretching modes have small but negative mode Grüneisen parameters. The Grüneisen parameters of the lattice modes of I_2O_5 are usually larger than 1 and also significantly larger than those of other modes. This reflects the fact that inter-molecular distances are greatly reduced by pressure.

Compared to solid I_2O_5, I_2O_6 has different vibrational properties. For example, the single bond stretching modes are not separated clearly from the deformation modes. Furthermore, the highest two stretching modes due to doubly bonded oxygen have frequencies far larger than the other modes, which lead to a broad gap in the phonon DOS (see Figs. 7 and 8). Again, these modes must be assigned to terminal I-O groups. These are also the only two modes with small negative Grüneisen parameters. As in I_2O_5, the Grüneisen parameters of the lattice modes are usually larger than 1, which is also the case for most other modes. Since the calculation also overestimates the bond lengths of I_2O_6, we believe that the frequencies of the stretching modes are also underestimated in our calculation.

Raman this study		exp.	infrared this study		exp.	Assignment
766.22	A_g	834				O3-I1-O2 st + O4-I2-O3 st
756.05	B_g	831	756.73	A_u	835	I2-O4 st
			754.61	B_u	820	IO_3 st
738.01	B_g	810				O1-I1-O2 st
			724.11	A_u	800	I1-O2 st
703.77	A_g	748				I1-O2 st + I2-O4 st
			704.19	B_u	755	O1-I1-O2 st + I2-O4 st
638.28	B_g	724				O3-I1-O1 st + IO3 (I2) asym. st
			691.02	B_u	720	I1-O1 + I2-O5 st
607.23	A_g	693				IO_3 (I1) asym.st + I2-O3 st
			594.59	B_u	670	O3-I2-O5 st + O2-I1-O3 asym. st
583.12	B_g	607				IO_3 asym.st + O3-I2-O5 st
			592.16	A_u	587	O1-I1-O3 asym.st + I2-O3 st
577.21	A_g	535	567.43	A_u	510	O3-I1-O1 st + O5-I2-O3 asym st
473.51	A_g	433	483.98	A_u		I2-O5 st
442.25	B_g	412				O3-I2-O5 asym. St + O3-I1st
			435.45	B_u	415	O3-I2-O5 asym. St + O3-I1-O1 asym. st
418.53	B_g	401	401.82	B_u		O5-I2-O4 bend
391.62	A_g		395.78	A_u		IO_3 bend
386.30	B_g	377	381.86	B_u		IO_3 bend
364.68	B_g	361	354.57	A_u	357	IO_3 bend
357.94	A_g		336.25	B_u	340	IO_3 bend
343.13	A_g		319.62	A_u	327	IO_3 bend
316.24	B_g	323	306.59	B_u	305	IO_3 bend
315.87	A_g		302.36	A_u		IO_3 bend
291.25	B_g	300	292.85	B_u		IO_3 bend
283.48	A_g		283.46	A_u	276	IO_3 bend
267.43	B_g		263.05	B_u		IO_3 bend
260.54	A_g	263	258.87	A_u		IO_3 bend
254.19	B_g		256.37	B_u		IO_3 bend (I1) +IO_3 rock (I2)
216.99	B_g		217.77	A_u	222	IO_3 bend (I1) + IO_3 rock (I2)
216.28	A_g		217.51	B_u		IO_3 bend
202.35	A_g	202	202.28	A_u	205	IO_3 bend
193.97	B_g	193				IO_3 rock
183.70	A_g		177.40	A_u	180	IO_3 bend (I2) + IO_3 rock (I1)
174.17	B_g	176	172.79	B_u		IO_3 rock
159.17	A_g		153.53	B_u		IO_3 rock
			152.49	A_u	153	IO_3 rock (I1)+IO_3 bend (I2)
151.76	B_g	146				lattice libration
			136.45	B_u		IO_3 rock (I2)+IO_3 bend (I1)

Raman this study		exp.	infrared this study		exp.	Assignment
142.63	A_g					IO_3 rock (I1)+IO_3 bend (I2)
125.95	A_g		131.78	A_u		IO_3 rock
			124.17	A_u	122	lattice libration
112.67	B_g	109	114.99	B_u		lattice libration
107.02	A_g					lattice translation
102.61	B_g	97	110.14	A_u	109	lattice translation
			92.58	A_u		lattice libration
83.60	B_g		91.72	B_u	87	lattice libration
83.52	A_g	80	78.55	B_u	81	lattice libration
64.58	B_g	65				lattice translation
			64.06	A_u	60	lattice libration
60.76	A_g	59				lattice translation
50.36	A_g					lattice translation
42.34	B_g	47				lattice libration

Figure 7. Vibrational modes of I_2O_5.

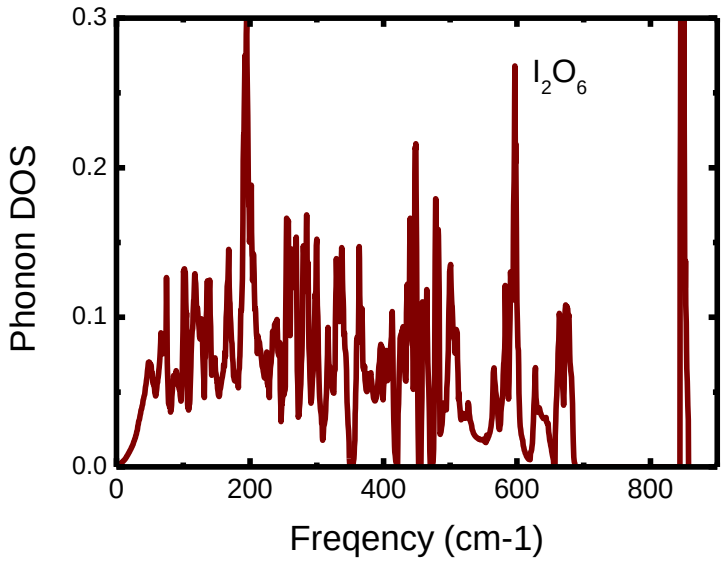

Figure 8. Phonon density of states of I_2O_6.

Raman	Infrared	assignment
843.9	844.8	I-O st (I1-O2, I2-O11)
675.8	660.3	IO_6 st
602.3	619.8	IO_6 st
594.5		IO_2 sci (O8-I3-O5, O18-I4-O19)
	562.5	IO_2 rock (O8-I3-O5, O18-I4-O19)
499.4		IO_2 asy st (O6-I3-O3, O7-I4-O10)
	519.8	IO_2 asy st (O6-I3-O3, O7-I4-O10), IO_2 bend (O8-I3-O5, O8-I4-O5)
487.5		IO_2 asy st (O9-I3-O12, O4-I4-O1)
	503.0	IO_2 asy st (O9-I3-O12, O4-I4-O1), IO_2 bend (O8-I3-O5, O8-I4-O5)
474.6		IO_2 rock (O8-I3-O5, O18-I4-O19)
	462.9	IO_2 asy st (O3-I3-O12, O10-I4-O1), IO_2 bend (O8-I3-O5, O8-I4-O5)
437.0		IO_2 rock (O1-I1-O3, O10-I2-O12), IO_2 rock (O8-I3-O5, O8-I4-O5)
	444.7	IO_2 sci (O1-I1-O3, O10-I2-O12), IO_2 bend (O8-I3-O5, O8-I4-O5)
433.9		IO_2 sci (O1-I1-O3, O10-I2-O12),
	403.6	IO_2 rock (O1-I1-O3, O10-I2-O12),
375.6		IO_3 rock (I1,I2), IO_2 sci (O7-I4-O4,O9-I3-O6)
	369.2	ring bend (I3-O8-I4-O5){folding}
346.4		ring rock (I3-O8-I4-O5), IO_3 bend (I1,I2),
	358.1	IO_3 rock (I1,I2), IO_2 sci (O7-I4-O4,O9-I3-O6)
342.6		IO_3 rock (I1,I2),
	319.2	ring (I3-O8-I4-O5) bend {folding}, IO_3 bend (I1,I2)
289.4		IO_3 st (I1,I2), IO_2 rock (O7-I4-O4,O9-I3-O6) {out of I_2O_4 plane}
	291.9	IO_3 bend (I1,I2), IO_2 rock (O7-I4-O4,O9-I3-O6) {in I_2O_4 plane}
284.4		IO_2 rock (O7-I4-O4,O9-I3-O6) {in IO_2 plane}, IO_2 rock (I1-O3-O1, I2-O10-O12)
	267.5	IO_2 rock (O7-I4-O4,O9-I3-O6){out of IO_2 plane}, IO_2 rock(I1-O3-O1, I2-O10-O12)
259.6		ring rock (I3-O8-I4-O5), IO_3 bend
	236.9	IO_2 rock (I1-O3-O1, I2-O10-O12), IO_2 sci (O7-I4-O4,O9-I3-O6)
223.3		wagging (I2-O11, I1-O2)
	213.7	IO_3 bend
214.3		IO_3 rock
	208.6	wagging (I2-O11, I1-O2)
206.1		wagging (I2-O11, I1-O2)
	197.6	ring bend (I3-O8-I4-O5) {folding}, IO_2 rock (O2-I1-O3, O11-I2-O10)
200.7		IO_3 bend
	174.5	IO_3 rock
189.9		IO_2 rock (O7-I4-O4,O9-I3-O6) {in I_2O_4 plane}
	154.1	IO_3 rock
136.3		IO_2 bend (I1-O3-O1, I2-O10-O12)
	139.2	IO_3 rock
120.6		lattice modes
99		lattice modes
81.1		lattice modes

Figure 9. Vibrational modes of I_2O_6.

III. Equation of States and Thermodynamic Properties

The equation of states of I_2O_5 and I_2O_6 are shown in Figs. 10 and 11. The calculation without VDW correction overestimates the volume significantly. However at high pressures, the effect of VDW on volume becomes less for both crystals. The volume differences between calculations with and without VDW correction for I_2O_5 and I_2O_6 at 0 GPa are 12.0% and 13.2%, respectively. At 5 GPa, these differences decrease for

I_2O_5 and I_2O_6 to 4.5% and 5.7%, respectively. The tendency that the VDW effect decreases with pressure is consistent with previous results for several other molecular crystals.

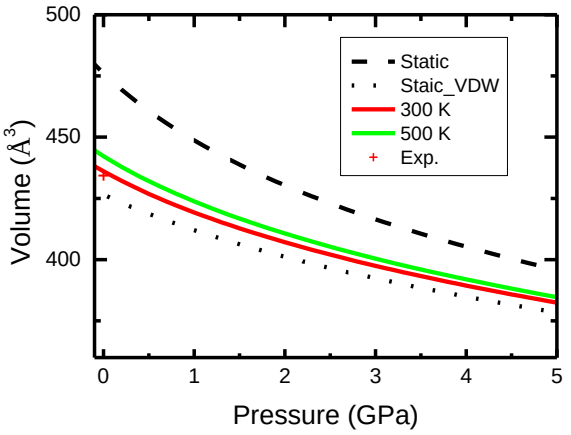

Figure 10. Equation of states of I_2O_5.

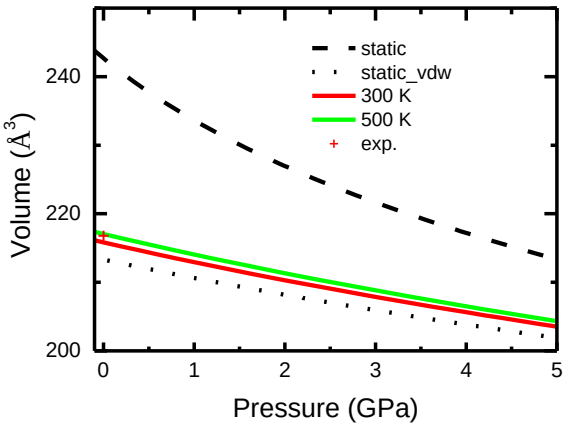

Figure 11. Equation of states of I_2O_6.

Vibrational contributions increase the equilibrium volume noticeably. For I_2O_5 and I_2O_6, the effect of zero-point motion and room temperature shifts the equilibrium volume by 2.2% and 0.9%, respectively. Interestingly, these values are very similar to those of materials such as MgO and Mg_2SiO_4, although the bulk moduli of MgO and Mg_2SiO_4 (at about 170 GPa) are far larger than those of iodine oxide crystals (at about 30 GPa). The

calculated equilibrium volume including VDW and phonon contributions agrees well with the experimental data (with differences smaller than 0.5%). The resulting equation of states provides reliable volumes at high pressure and temperature.

Thermodynamic properties of two crystals including thermal expansion, heat capacity, adiabatic bulk modulus and thermal Grüneisen parameters are shown in Figs. 12 and 13.

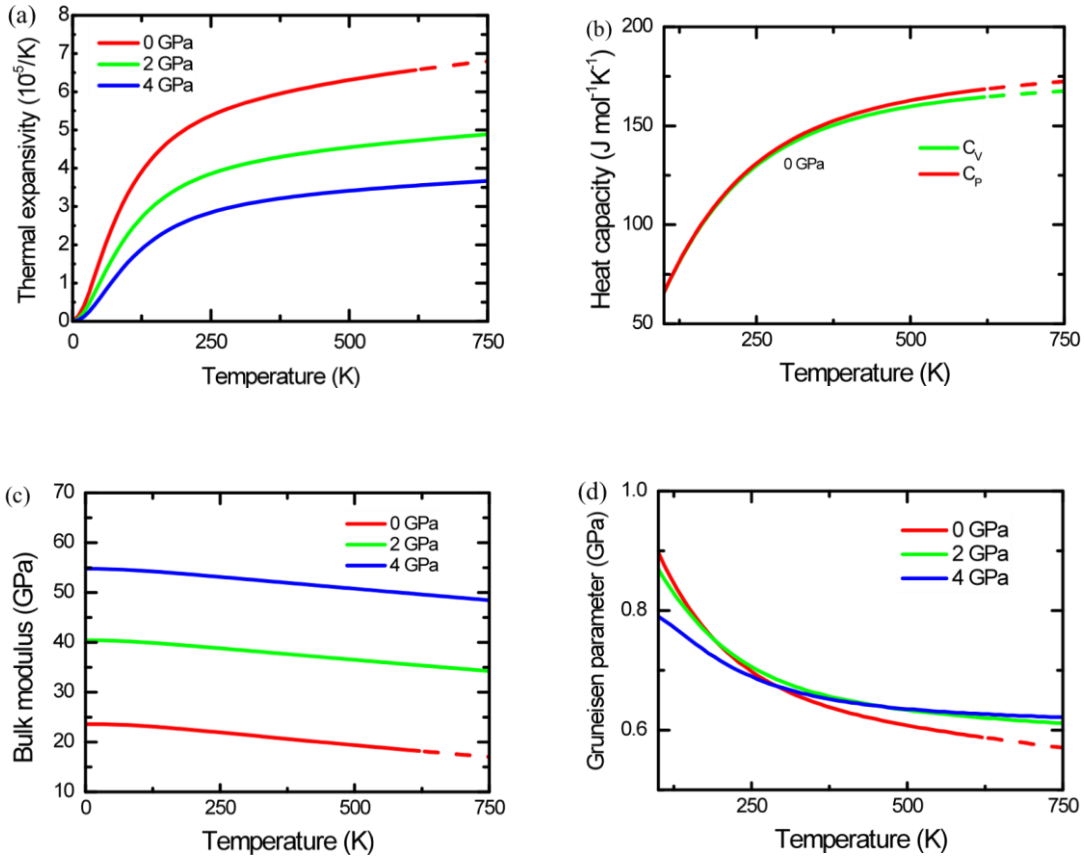

Figure 12. Thermodynamic properties of I_2O_5: (a) thermal expansion, (b) heat capacity at constant pressure C_P and volume C_V, (c) adiabatic bulk modulus, and (d) Grüneisen parameters.

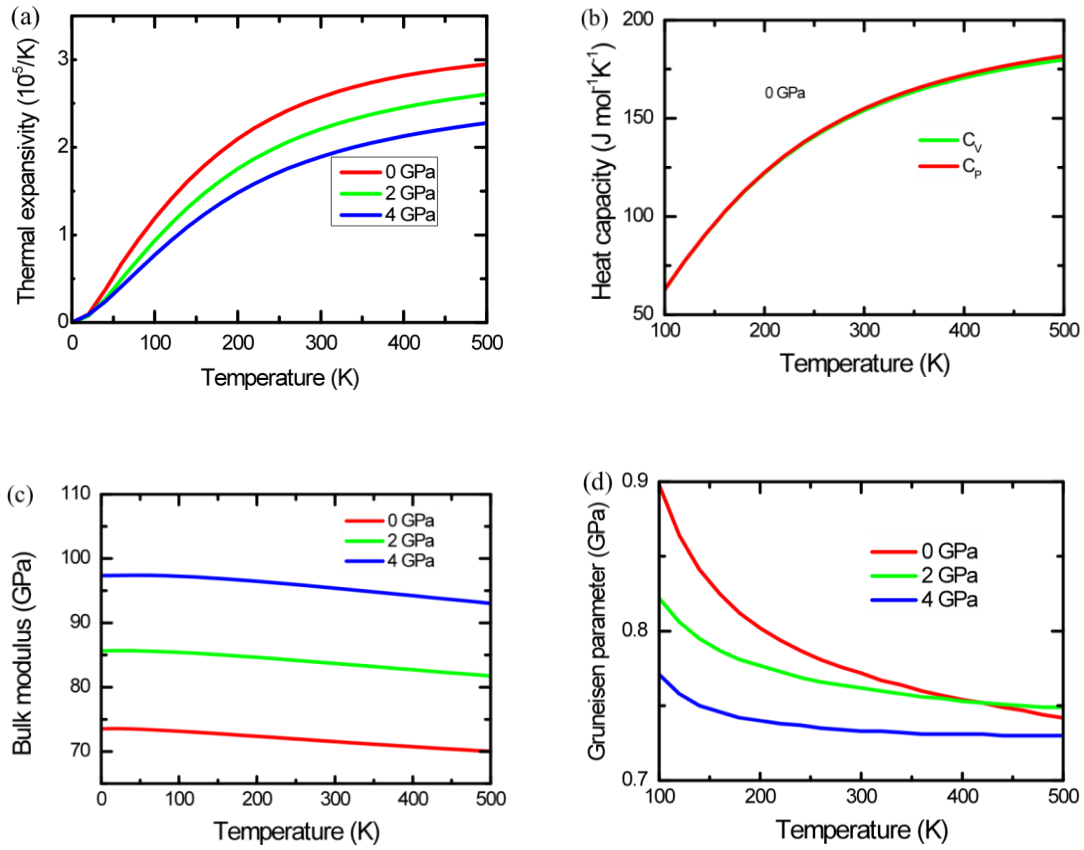

Figure 13. Thermodynamic properties of I_2O_6: (a) thermal expansion, (b) heat capacity at constant pressure C_P and volume C_V, (c) adiabatic bulk modulus, and (d) Grüneisen parameters.

The thermal expansion coefficient increases rapidly at low temperatures up to about 250K and then increases slightly with increasing temperature. The bulk modulus decreases almost linearly with temperature. The thermal Grüneisen parameter, which is defined as $\gamma_{th} = \alpha K_T V / C_V$, is the weighted average of the mode Grüneisen parameters. At low temperatures, the thermal Grüneisen parameter is determined mostly by the low frequency modes. With increasing temperature, all modes tend to contribute evenly and, hence, the thermal Grüneisen parameter is close to the average value of the mode Grüneisen parameters. Therefore the thermal Grüneisen parameter is almost temperature independent at sufficiently high temperatures. Low frequency modes (lattice modes) have

larger Grüneisen parameters than other modes, and this explains why the thermal Grüneisen parameters decrease with temperature.

The heat capacity at constant pressure, C_P, and constant volume, C_V, are related by $C_P = (1 + \alpha\gamma_{th}T)C_V$. Heat capacity increases rapidly below about 250K and tends to saturate at high temperatures. Since we use a quasi-harmonic approximation in the calculation, C_V is subjected to the law of Dulong and Petit. However, C_P can be significantly larger than the Dulong and Petit limit.

IV. Neutron Scattering Results

Neutron diffraction and inelastic scattering experiments were done in collaboration with the Spallation Neutron Source at Oak Ridge (Dr. Alexander Kolesnikov) and the NIST Reactor (Dr. Yun Liu). Diffraction measurements at low temperature were completed. Analysis of the inelastic neutron measurements has also been completed. The results from these studies have been summarized in the following manuscript for publication.

Phonon Density of States of Iodine Oxides – I_2O_5 and I_2O_6: A Joint Study Using Neutron Scattering and First-principles Calculations

A. I. Kolesnikov,[1] D. L. Abernathy,[1] A. Huq,[1] J. P. Hodges,[1] G. E. Granroth,[1] C.-K. Loong,[2] K. O. Christe,[3] R. Haiges,[3] R. K. Kalia,[4] A. Nakano,[4] K. Nomura, [4] P. Vashishta,[4] and Z.-Q. Wu[4]

[1]*Neutron Scattering Sciences Division, Oak Ridge National Laboratory, Oak Ridge, TN 37831-6473, USA*

[2]*School of Physics and Engineering, Sun Yat-Sen University, Guangzhou, 510275, China*

[3]*Loker Research Institute and Department of Chemistry, University of Southern California, Los Angeles, CA 90089-1661, USA*

[4]*Collaboratory for Advanced Computing and Simulations, University of Southern California, Los Angeles, CA 90089-0242, USA*

Iodine oxides I_2O_y (y = 4, 5 and 6) crystallize into atypical structures that fall in between the molecular- and framework-base types and exhibit high reactivity in ambient environment. We performed neutron, Raman and IR measurements of the crystal structures and lattice dynamics of newly synthesized, pure I_2O_5 and I_2O_6 samples. The molecular units within the crystals, their connectivity with neighboring units to form chain-like or framework-like structures, and the intra-and inter-molecular vibrations and phonon densities of states were characterized. The experimental information enables the systematic optimization of the structures and dynamics of the three oxides, I_2O_4, I_2O_5 and I_2O_6, by first-principles calculations. The van der Waals interaction as a crucial factor in the optimization process on top of the density functional theory was revealed through a quantitative comparison of the calculated crystal structures and phonon densities of states with experiments. These results permit the calculations of the equations of states, bulk modulus, thermal Grüneisen parameters, and other physical quantities that are useful for further understanding of the thermodynamic properties of iodine oxides under extreme conditions.

Iodine oxides play a critical role in many important physiochemical phenomena and, once their basic thermodynamic and chemical properties are understood, may lend themselves to a series of overarching technological applications. Firstly, iodine oxides, generated by photolysis of biogenic iodocarbons emitted from marine algae, interacts with O_3 under ultraviolet radiation to produce aerosol and cloud condensation nuclei, hence contributing to climate change [1, 2]. Secondly, iodine oxides are versatile and effective oxidants. For example, I_2O_5 is known to the oxidation of alcohol, the nine-membered amide and cycloalkan[*b*]indoles whereby useful products can be synthesized in atom-efficient, chemoselective, and environmental friendly way [3, 4]. Finally, I_2O_6 and I_2O_7 are predicted to be effective neutralizing reagents that defeat the functionality of chemical and biological agents.

Notwithstanding a long history of research, experimental characterization of iodine oxides has been limited mainly to I_2O_4, I_2O_5, and a few intermediate compounds associated with interactions with water and sulfuric acid. *Ab initio* calculations have been performed in various molecular iodine oxides, INO_3, HOI species [5, 6], but apparently no rigorous calculation of the structural and thermodynamic properties of bulk I_2O_4, I_2O_5 and I_2O_6 has appeared in the literature. Among the I_2O_y (y = 4-7) materials, the crystal structures of the y = 4, 5 and 6 members are found to conform to the trend of changing from polymeric-like to framework-like structures with increasing oxygen content. Consequently, the thermodynamic properties of I_2O_6, particularly under high-pressure and high-temperature conditions, are expected to differ from those of I_2O_4 and I_2O_5. To this end, the properties of I_2O_6 are of most interest, but chemical instability of this material has precluded the synthesis of bulk I_2O_6, let alone experimental characterization. In this paper, we present a joint neutron-diffraction/spectroscopic plus Raman/IR measurements and first-principles calculation of the structure, phonon density of states, and thermodynamic properties of bulk, anhydrous I_2O_y. The theoretical results are compared with the experimental neutron, Raman, and IR data in the literature as well as from present measurements. With both the structure and lattice dynamics optimized, we carried out calculations of the equations of states and other thermodynamic properties of the three iodine oxides.

The previously in the literature described methods for the synthesis of I_2O_6 have serious drawbacks. The thermal decomposition of H_5IO_6 in a vacuum [7] is difficult to control and produces I_2O_6 that is contaminated with side products. Furthermore, this preparation is only applicable for very small amounts of material. While the dehydration of H_5IO_6 in concentrated H_2SO_4 at 70 °C was reported to proceed only very slowly during the course of one month [8], dehydration of a mixture of H_5IO_6 and HIO_3 with 65% oleum resulted in impurities of $(IO_2)_2S_2O_7$ [9]. During the course of our study, it was found that the dehydration of a mixture of H_5IO_6 and HIO_3 with a stoichiometric amount of SO_3 in 100% sulfuric acid at elevated temperature yields pure I_2O_6 on a several gram scale within a few hours:

$$H_5IO_6 + HIO_3 + 3SO_3 \xrightarrow{H_2SO_4} I_2O_6 + 3H_2SO_4 \qquad (1)$$

An excess of SO_3 should be avoided because it will result in the formation of $(IO_2)_2S_2O_7$. The sulfuric acid can be removed by washing with anhydrous trifluoroacetic acid under anhydrous conditions.

During the course of this study, it was found that commercially available samples of I_2O_5 were not suitable for the neutron experiments because they contained small amounts of hydrogen containing compounds. These not further identified impurities could not be removed by heating the samples to 200 °C in a vacuum for 36 hours. Pure I_2O_5 suitable for the neutron experiments was then prepared by the thermal decomposition of I_2O_6:

$$2I_2O_6 \xrightarrow{130\text{ to }170°C} 2\ I_2O_5 + O_2 \qquad (2)$$

This is an exothermic reaction and care must be taken to remove the heat of reaction, especially for large reaction batches. Otherwise, the reaction mixture can overheat which results in thermal decomposition of I_2O_5 to I_2. Such an event was observed by us when a 250 mL glass flask loaded with 10 mmol of I_2O_6 was heated to 145 °C in an oil bath, resulting in a run-away exothermic decomposition reaction resulting in partial decomposition of I_2O_5 to I_2.

All reactions were carried out under dry nitrogen using standard Schlenk techniques. Non-volatile materials were handled in the dry nitrogen atmosphere of a glove box. Glassware was heated out under vacuum before use. Raman spectra were recorded directly in the Teflon reactors in the range 4000–80 cm^{-1} on a Bruker Equinox 55 FT-RA spectrophotometer, using a Nd-YAG laser at 1064 nm with power levels of 200 mW.

Infrared spectra were recorded in the range 4000-400 cm^{-1} on a Midac, M Series, FT-IR spectrometer using KBr pellets. The pellets were prepared inside the glove box using an Econo mini-press (Barnes Engineering Co.) and transferred inside a closed container to the spectrometer before placing them quickly into the sample compartment, which was purged with dry nitrogen to minimize exposure to atmospheric moisture and potential hydrolysis of the sample. The starting materials HIO_3, H_5IO_6, H_2SO_4 and oleum (all Aldrich) were used without further purification. Trifluoroacetic acid (SynQuest Labs, Alachua, FL) was freshly destilled from P_2O_5 prior to use. I_2O_6 was prepared by a modified literature synthesis [8, 9]. I_2O_5 was prepared by thermal decomposition of I_2O_6. The purity of the I_2O_6 and I_2O_5 samples was checked by their Raman and IR spectra.

Preparation of diiodine(V,VII)oxide, I_2O_6

Finely ground HIO_3 (100.41 g, 0.571 mol) and H_5IO_6 (130.10 g, 0.571 mol) were loaded into a Schlenk flask and conc. sulfuric acid (400 mL) was added. The mixture was heated to 90 °C and stirred. After about 15 minutes, a yellow suspension has formed. The flask was now removed from the heat source and 30% oleum (184 mL) was added under vigorous stirring to the hot suspension. The mixture was stirred at ambient temperature for 16 hours. The mixture was filtered through a fine porcelain filter frit and the yellow solid washed ten times with 200 mL of dry trifluoroacetic acid. The solid was then dried in a vacuum at ambient temperature for 14 hours. We thus obtained 197.2 g of finely powdered, yellow I_2O_6 (weight expected for 0.571 mol I_2O_6: 199.7 g).

Preparation of diiodine(V)oxide, I_2O_5

I_2O_6 (2.50 g, 7.15 mmol) was loaded into a glass ampule equipped with a grease-less Kontes HiVac valve with a Teflon stopcock. After the ampule was evacuated, the valve was closed and the vessel placed in an oil bath at ambient temperature. The bath was then heated to 130 °C. After 30 minutes, the temperature was raised to 150 °C. After another 30 minutes, the temperature was raised to 160 °C and after another 30 minutes, raised to 170 °C. The solid was kept at this temperature for 12 hours after which it had turned completely white. The ampule was allowed to cool to ambient temperature and connected to a glass vacuum line. The amount of non-condensible gas produced inside the ampule was determined by p, V, and T measurements to 7.2 mmol). We thus obtained 2.34 g of finely powdered, white I_2O_5 (weight expected for 7.15 mmol I_2O_5: 2.39 g).

The crystal structures of anhydrous I_2O_4 and I_2O_5 over the temperature range of 4-300 K were investigated by neutron powder diffraction using the POWGEN facility at the Spallation Neutron Source (SNS) of Oak Ridge National Laboratory. Inelastic neutron scattering was carried out at low temperature (10 K) using the chopper spectrometer, ART, also at SNS [ref]. The samples were sealed inside a helium-filled container throughout the experiments to avoid interaction with the ambient atmosphere. The extraordinary large neutron incoherent scattering cross section from hydrogen, during a long run, serves as a sensitive tester of the presence of water or H-containing impurities. We find no evidence of incoherent-scattering background or local-mode vibrations due to hydrogen species in the samples.

Owing to the larger size and more polarizable orbitals of the I atom than those of the O atom, the binary system of I_2O_y accommodates the increasing oxygen content structurally via adjustments of the coordination numbers of the I atoms and the I-O-I bond angles but always stay in between the molecular- and framework-type crystal structures. Figures 1 (a)-(c) illustrates the molecular units in the I_2O_4 (monoclinic, $P2_1/c$, Z = 4), I_2O_5 (monoclinic, $P2_1/c$, Z = 4), and I_2O_6 (triclinic, $P\bar{1}$, Z = 2) in the crystal. In all cases, neighboring molecules are connected by some intermolecular I-O bonds (2.05-2.9 Å) that are significantly shorter than the van der Waals (vdW) distance (~3.5 Å). Furthermore, each structure preferably features longer intermolecular I-O bonds along a crystallographic direction, *i.e.*, $\vec{b}$, $\vec{c}$, and $\vec{a}$ directions for I_2O_4, I_2O_5, and I_2O_6, respectively. H_2O or SO_4 acid molecules tend to enter the lattice, forming inserted layered structures to break up the IO_x framework, thereby rendering the I_2O_y system thermodynamically unstable.

Computations were performed using the Quantum ESPRESSO [10], a package based on the density functional theory (DFT), plane wave, and pseudopotential. The pseudopotential for I and O atoms were generated by the method of Troullier and Martins [11] in conjunction with the generalized-gradient approximation (GGA) for the exchange-correlation functionals [12]. To account for the VDW interaction between molecules, an empirical VDW correction proposed by Grimme was incorporated [13]. The dispersion correction is given by

$$E_{\text{disp}} = -s_6 \sum_{i<j} \frac{C_{ij}}{R_{ij}^6} f_{\text{damp}}(R_{ij}), \quad (3)$$

where C_{ij} and R_{ij} denote the dispersion coefficient and interatomic distance between the i^{th} and j^{th} atoms, s_6 is a global scaling factor that depends only on the density functional. A damping function, f_{damp}, is introduced to ensure that the dispersion correction is negligible for small R_{ij}. During the structural optimization using the scheme of damped variable-cell-shape molecular dynamics (MD) [14], vdW corrections have to be introduced to bring the lattice constants matching the experimental values. The final optimization introduced as much as 5-8% corrections for the *b*, *c*, and *a* lattice constant of I_2O_4, I_2O_5 and I_2O_6, respectively, and about one third of these values for other lattice constants. Specifically, we have to modify the global scaling factor from its nominal value of s_6 = 0.75, to 1.0 and 2.0 respectively for I_2O_5 and I_2O_6 in order to account for their experimental unit-cell volumes. This anisotropy results from the tight molecular netting in the *ac*, *ab*, and *bc* planes in the I_2O_4, I_2O_5 and I_2O_6 structures, respectively, see Figs. 1 (a)-(c). This characteristic is corroborated by experiments, for example, through the anisotropic thermal expansion of the I_2O_6 lattice favoring the $\vec{a}$ direction as observed by neutron diffraction (Fig. 1 (d)). Due to the large difference in the atomic size between I and O, the theoretical implement of the VDW correction has a non-trivial impact on the bond lengths and bond angles. In general, the intermolecular bond lengths agree with experimental values, but the intramolecular bond lengths are overestimated by 2-3% and up to ~5% in some cases.

Dynamically, the effect of VDW forces correlates not only with the variation of the vibrational frequencies but also more rigorously with the phonon density of states (PDOS). Therefore, a quantitative comparison of the combined structural and dynamic data with first-principles calculations permits a systematic assessment of the interplay between atomic/molecular forces and the structural/thermodynamic properties. The phonon calculation is performed by a diagonalization of the dynamical matrices first computed on a 2×2×2 and later interpolated to a 6×6×6 mesh in the first Brillouin zone

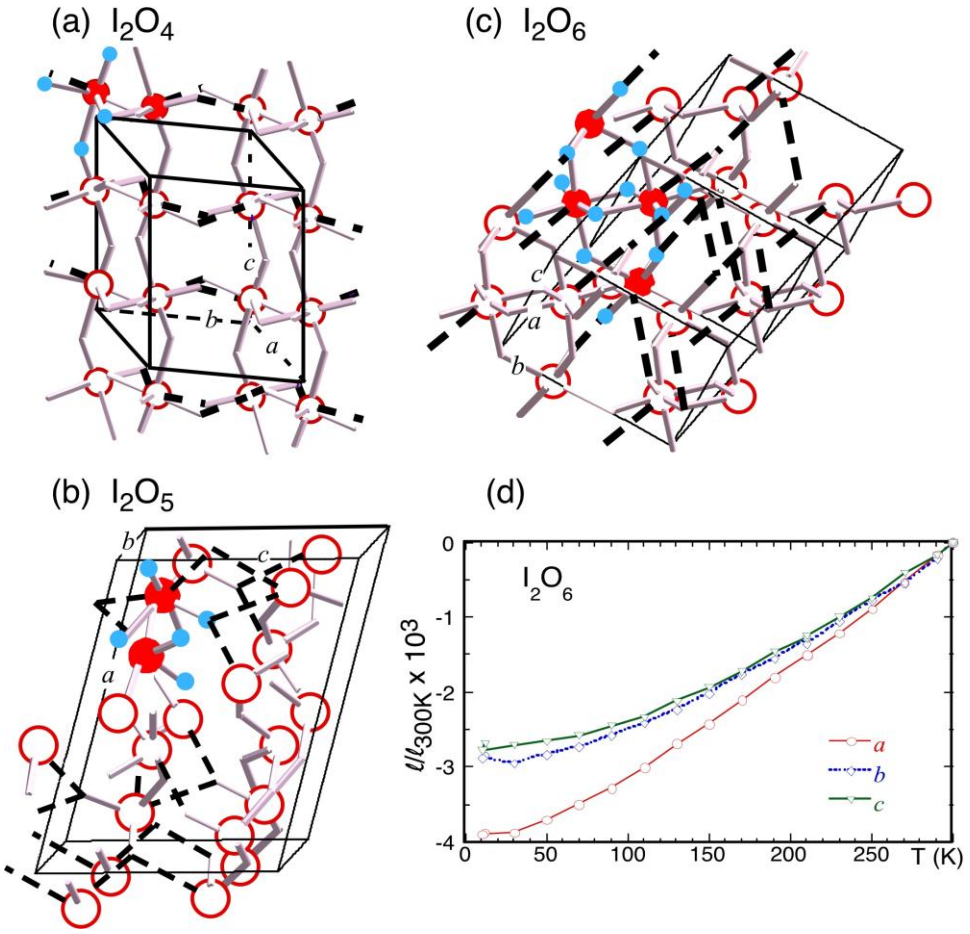

FIG. 1. (a-c): The crystal structures of I_2O_y (y = 4, 5, and 6), where the unit cells are outlined by solid lines and the molecular units, I_2O_4, I_2O_5, and I_4O_{12}, are identified by atoms denoted in solid circles (large I, small O). The molecular chain along the c-direction in I_2O_4, layer-like substructure in the ab-plane in I_2O_5, and framework configuration in I_2O_6 are noticeable. This in turn favors the formation of longer and weaker intermolecular I-O bonds (dashed lines) along the $\vec{b}$, $\vec{c}$, and $\vec{a}$ directions for I_2O_4, I_2O_5 and I_2O_6, respectively, as is also evident as anisotropic vdW interaction in the molecular-dynamics simulation. (d) The change in the lattice parameters of I_2O_6 relative to those at 300K, showing a softer c-direction.

using density functional perturbation theory [15] and the visualization of the lattice-, intermolecular- and intramolecular vibrational modes by the Molden-4.7 software. Inelastic neutron scattering, on the other hand, measures the neutron-weighted (NW) PDOS according to

$$G(E) = \frac{2\bar{M}}{\hbar^2}\left\langle \frac{e^{2W(Q)}}{Q^2}\frac{E}{n+1}S(Q,E)\right\rangle \propto \bar{M}\sum_i \frac{c_i s_i}{M_i}F_i(E) \qquad (4)$$

where c_i, σ_i, M_i, and $F_i(E)$ are the concentration, scattering cross section, mass and partial PDOS, respectively, for the i^{th} atomic species. $\bar{M}$ is the mean sample mass, n is the Bose population factor, and $S(Q, E)$ is the observed neutron scattering function for one-phone excitations as a function of energy E and wavevector Q. The Debye-Waller factor $e^{2W(Q)} \approx aQ^2$ for one-phonon processes can be estimated from diffraction data. $\langle ... \rangle$ and represents the average over a wide range of observed Q values. The experimental NWPDOS is compared with that obtained from Eq. (4) using the $F_i(E)$ from MD simulations convoluted with the instrumental resolution function.

The calculated and measured NWPDOS for I_2O_5 and I_2O_6 as well as the experimental Raman and IR frequencies are shown in Fig. 2. Firstly, the lattice modes below ~15 meV extend to the internal molecular vibrations of higher energies without obvious division, reflecting the comparable bond strengths connecting the atoms within the I_2O_4, I_2O_5, and I_4O_{12} units and the atoms between neighbor molecules. For I_2O_4 (not shown) and I_2O_5, there is a ~10 meV wide gap at around 60 meV dividing the bending/rocking modes and the stretch vibrations, but for I_2O_6 such gap does not exist. Moreover, the 1-phonon cutoff is seen at 103, 109, and 114 meV for I_2O_4, I_2O_5 and I_2O_6, respectively. These observations are consistent with the stiffening of the lattice by the stronger framework-like connection of the molecular units with increasing oxygen content. Secondly, while the Raman and IR zone-center modes agree well with the neutron peak positions, the calculated NWPDOS shows some marked differences. For example, For I_2O_5 the calculation predicted higher upper frequencies of molecular bending modes and lower stretch mode energies than the observed values. This is not surprising because the stretch modes are sensitive to the bond lengths; their low values are the direct result of the overestimated intramolecular I-O bond lengths resulted from the vdW correction. Likewise, the vdW correction underestimated the short intermolecular I-O bond lengths hence the higher predicted frequencies of the upper bending modes. This happens also in the case of I_2O_4 through an examination of the calculation PDOS and the Raman and IR frequencies [11, Ellestad *et al.*]. For I_2O_6 the calculated I-O band-stretching frequencies are clearly underestimated but the framework-like crystal structure apparently harden the bending modes thereby filling the gap that is seen in I_2O_4 and I_2O_5. Finally, the observed

phonon spectra are not as sharp as the calculated ones perhaps due to the combination of residual multi-phonon and small-size crystallite broadening effects.

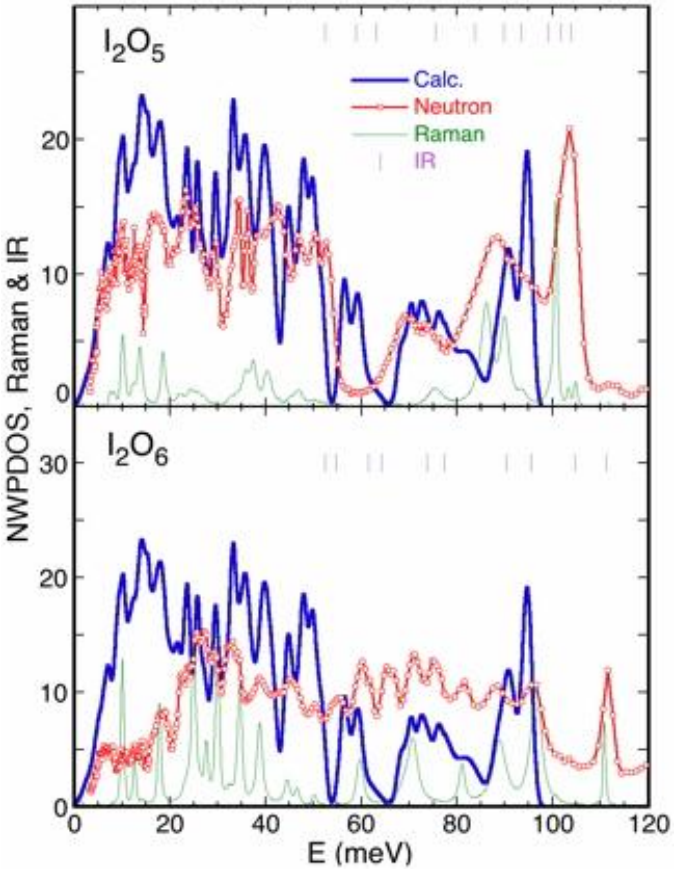

FIG 2. The measured and calculated neutron-weighted phonon densities of states for I_2O_5 and I_2O_6 that are normalized to have the same integrated area, and the Raman and IR data. The observed IR frequencies about 50 meV are represented by tick marks and the measured Raman spectra are displayed in arbitrary units.

The MD simulations account reasonably well the crystal structures and lattice dynamics of the I_2O_y system notwithstanding the 10-15% energy shifts of the high-energy modes caused by the compromise between inter- and intramolecular interactions from the VDW correction. We have calculated the equation of state, thermal expansion, heat capacity, adiabatic bulk modulus and thermal Grüneisen parameters (the weighted average of the mode Grüneisen parameters) for I_2O_4, I_2O_5 and I_2O_6. Figure 3 shows the effects on the calculated equations of state: the substantial overestimation without the vdW correction and the adjustment of the s_6 parameter, and the improvement by including the thermal contribution of phonons under the quasi-harmonic approximation.

The contribution of thermal vibrations (including the zero-point motion) to the equilibrium volume as a function of pressure is evident and amounts to about 0.9 to 2.2%. Interestingly, these values are comparable to those of MgO and Mg_2SiO_4 [16] in spite of the large difference in the bulk modulus between the latter 3D framework crystals (~170 GPa) and the iodine oxides (~30 GPa). The three iodine oxides have similar thermal pressure gradient of ~1.7 GP/1000K. As a result, the magnitude of the bulk modulus, $a_{I_2O_5} > a_{I_2O_4} > a_{I_2O_6}$, follows the order of the density, $r_{I_2O_5} > r_{I_2O_4} > r_{I_2O_6}$.

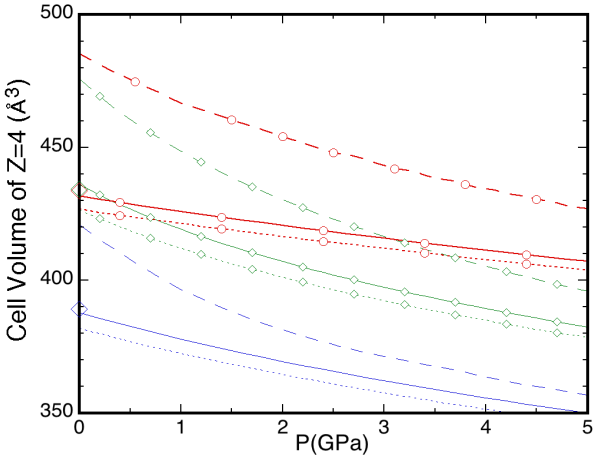

FIG 3. The calculated equations of state for I_2O_4 (lines), I_2O_5 (lines affixed with diamonds), and I_2O_6 (lines affixed with circles). For each I_2O_y member calculations without vdW force corrections (dashed lines), with vdW force correction but not including thermal contribution from phonons (dotted lines), and with both vdW force correction and phonon contributions at 300K (solid lines) are shown. Experimental cell volumes for 4 formula units at ambient pressure are shown by large diamonds.

In summary, neutron, Raman and IR measurements of the crystal structures, vibrational mode frequencies, and phonon densities of states of newly synthesized pure, anhydrous I_2O_5 and I_2O_6 samples provided the crucial experimental data for the optimization of both the structures and dynamics of I_2O_4, I_2O_5, and I_2O_6 via *ab initio* MD simulations. Important thermodynamic properties were computed for further understanding of the materials under extreme conditions.

We thank Yun Liu for his assistance in obtaining some initial neutron-diffraction data at the NIST facility. Work at ORNL was sponsored by the Scientific User Facilities Division, Office of Basic Energy Sciences, U.S. Department of Energy; ORNL is

managed by UT-Batelle, LLC, under contract DE-AC0500OR22725 for the U.S. Department of Energy. Research Work at USC was supported by the Defense Threat Reduction Agency (DTRA) -Basic Research.

References

[1] I. Pundt *et al.*, J Atmos Chem **30**, 173 (1998).

[2] R. Vogt *et al.*, J Atmos Chem **32**, 375 (1999).

[3] Z. Q. Liu *et al.*, Tetrahedron Lett **48**, 3017 (2007).

[4] K. Yoshida, J. Goto, and Y. Ban, Chem Pharm Bull **35**, 4700 (1987).

[5] B. Minaev *et al.*, Spectrochim Acta a **58**, 1039 (2002).

[6] N. Kaltsoyannis, and J. M. C. Plane, Phys Chem Chem Phys **10**, 1723 (2008).

[7] L. Pacesova, and Z. Hauptman, Z Anorg Allg Chem **325**, 325 (1963).

[8] T. Kraft, and M. Jansen, J Amer Chem Soc **117**, 6795 (1995).

[9] V. H. Siebert, M. Weise, and U. Woerner, Z Anorg und Allg Chem **432**, 136 (1977).

[10] P. Giannozzi *et al.*, J Phys-Condes Matter **21**, 395502 (2009).

[11] N. Troullier, and J. L. Martins, Phys Rev B **43**, 1993 (1991).

[12] J. P. Perdew, K. Burke, and M. Ernzerhof, Phys Rev Lett **77**, 3865 (1996).

[13] S. Grimme, J Comput Chem **27**, 1787 (2006).

[14] R. M. Wentzcovitch, Phys Rev B **44**, 2358 (1991).

[15] S. Baroni *et al.*, Rev Mod Phys **73**, 515 (2001).

[16] Z. Wu, and R. M. Wentzcovitch, J Geophys Res **112**, B12202 (2007).

Personnel Supported

Synthesis Task

The following people have been supported under the Synthesis Task:

K. O. Christe,

R. Haiges,

W. W. Wilson,

Guillaume Belanger-Chabot.

Simulation Task

Priya Vashishta,

Rajiv K. Kalia,

Aiichiro Nakano,

Zhongqing Wu,

Richard Clark.

Publications

- D. A. Dixon, D. J. Grant, K. O. Christe, and K. A. Peterson "The Structure and Heats of Formation of Iodine Fluorides and the Respective Closed Shell Ions from CCSD(T) Electronic Structure Calculations and Reliable Prediction of the Sterical Activity of the Free Valence Electron Pair in ClF_6^-, BrF_6^- and IF_6^-," Inorg. Chem., 47, 5485 (2008).
- K. O. Christe, "Neil Bartlett (1932-2008), Founder of Noble-Gas Chemistry," Nature, Vol. 455, 11 September, 2008.
- D. J. Grant, D. A. Dixon, D. Camaioni, R. G. Potter, and K. O. Christe, "Lewis Acidities and Hydride, Fluoride, and X^- Affinities of the $BH_{3-n}X_n$ Compounds for (X = F, Cl, Br, I, NH_2, OH, and SH) from Coupled Cluster Theory," Inorg. Chem., 48, 8811 (2009).
- K. O. Christe, R. Haiges, W. W. Wilson, and J. A. Boatz, "Synthesis and Properties of N_7O^+," Inorg. Chem., 49, 1245 (2010).

- D. J. Grant, T-H. Wang, D. A. Dixon, and K. O. Christe, "Heats of Formation of XeF_3^+, XeF_3^-, XeF_5^+, XeF_7^+, XeF_7^-, and XeF_8 from High Level Electronic Structure Calculations, Inorg. Chem., 49, 261 (2010).
- R. Craciun, D. Picone, R. T. Long, S. Li, D. A. Dixon, K. A. Peterson, and K. O. Christe, "Third Row Transition Metal Hexafluorides, Extraordinary Oxidizers and Lewis Acids: Electron Affinities, Fluoride Affinities, and Heats of Formation of WF_6, ReF_6, OsF_6, IrF_6, PtF_6, and AuF_6," Inorg. Chem., 49, 1056 (2010).
- R. Craciun, R. T. Long, D. A. Dixon, and K. O. Christe, "Electron Affinities, Fluoride Affinities, and Heats of Formation of the Second Row Transition Metal Hexafluorides: MF_6 (M = Mo, Tc, Ru, Rh, Pd, Ag)," J. Phys. Chem. A, 114, 7571 (2010).
- K. O. Christe, D. A. Dixon, D. J. Grant, R. Haiges, F. S. Tham, A. Vij, V. Vij, T.-H. Wang, and W. W. Wilson, "Dinitrogen Difluoride Chemistry. Improved Syntheses of *cis*- and *trans*-N_2F_2, Synthesis and Characterization of $N_2F^+Sn_2F_9^-$, Ordered Crystal Structure of $N_2F^+SbF_2F_{11}^-$, High-Level Electronic Structure Calculations of *cis*-N_2F_2, *trans*-N_2F_2, $F_2N{=}N$, and N_2F^+, and Mechanism of the *trans-cis* Isomerization of N_2F_2," Inorg. Chem., 49, 6823 (2010).
- K. O. Christe, A. Dixon, R. Haiges, M. Hopfinger, V. E. Jackson, T. M. Klapoetke, B. Krumm, and M. Scherr, "Selenium(IV) Fluoride and Oxofluoride Anions," J. Fluor. Chem., 131, 791 (2010).
- R. Haiges, J. A. Boatz, and K. O. Christe, "The Syntheses and the Structure of the First Vanadium(IV) and Vanadium(V) Binary Azides, $V(N_3)_4$, $[V(N_3)_6]^{2-}$ and $[V(N_3)_6]^-$," Angew. Chem. Int. Ed., 49, 8008 (2010).
- D. J. Grant, T-H. Wang, M. Vasiliu, D. A. Dixon, and K. O. Christe, "F^+ and F^- Affinities of Simple N_xF_y and O_xF_y Compounds," Inorg. Chem., 50, 1914 (2011).
- K. O. Christe, R. Haiges, J. A. Boatz, H. D. B. Jenkins, E. B. Garner, and D. A. Dixon, "Why Are $[P(C_6H_5)_4]^+N_3^-$ and $[As(C_6H_5)_4]^+N_3^-$ Ionic salts and $Sb(C_6H_5)_4N_3$ and $Bi(C_6H_5)_4N_3$ Covalent Solids? A Theoretical Study Provides an Unexpected Answer," Inorg. Chem., 50, 3752 (2011).
- R. Haiges, J. A. Boatz, J. M. Williams, and K. O. Christe, "Preparation and Characterization of the Binary Group 13 Azides, $M(N_3)_3$,and $M(N_3)_3{\cdot}CH_3CN$ (M =

Ga, In, Tl), $[Ga(N_3)_5]^{2-}$, and $[M(N_3)_6]^{3-}$ (M = In, Tl)," Angew. Chem. Int. Ed., 50, 8828 (2011).

- R. Haiges, M. Rahm, D. A. Dixon, E. B. Garner, III, and Karl O. Christe, "Binary Group 15 Polyazides. Structural Characterization of $[Bi(N_3)_4]^-$, $[Bi(N_3)_5]^{2-}$, $[bipy{\cdot}Bi(N_3)_5]^{2-}$, $[Bi(N_3)_6]^{3-}$, $bipy{\cdot}As(N_3)_3$, $bipy{\cdot}Sb(N_3)_3$, and $[(bipy)_2{\cdot}Bi(N_3)_3]_2$ and on the Lone Pair Activation of Valence Electrons," Inorg. Chem., 51, 1127 (2012).
- V. E. Jackson, D. A. Dixon and K. O. Christe, "Thermochemical Properties of Selenium Fluorides, Oxides and Oxofluorides," Inorg. Chem., 51, 2472 (2012).
- K. S. Thanthiriwatte, M. Vasiliu, D. A. Dixon and K. O. Christe, "Structural and Energetic Properties of Closed Shell XF_n (X = Cl, Br, and I; n = 1-7) and XO_nF_m (X = Cl, Br, and I; n = 1-3; m = 0-6) Molecules and Ions Leading to Stability Predictions for Yet Unknown Compounds," Inorg. Chem., 51, 10966 (2012).
- R. Haiges, M. Rahm and K. O. Christe, "Unprecedented Conformational Variability in Main Group Inorganic Chemistry: the Tetraazidoarsenite and –Antimonite Salts $A^+[M(N_3)_4]^-$ (A = NMe_4, PPh_4, $(Ph_3P)_2N$; M = As, Sb), Five Similar Salts, Five Different Anion Structures, Inorg. Chem., 51, XXXX (2012), in press.
- F. Shimojo, A. Nakano, R. K. Kalia, and P. Vashishta, "Density functional study of 1,3,5-trinitro-1,3,5-triazine molecular crystal with van der Waals interactions," *J. Chem. Phys.*, 132, 94106 (2010).

Interactions/Transitions

The following Conferences were attended and invited papers were presented:

Intersib Fluorine 2008, Vladivostok, Russia

Halchem IV, Platja d'Aro, Spain, 2008

Seminar, Universidad Autonoma, Barcelona, Spain, 2008

19th ACS Winter Fluorine Conference, St. Pete Beach, FL, 2009

Seminar, University of California, San Diego, CA, 2009

Jenkins Retirement Symposium, University of Warwick, Warwick, UK, 2009

2009 AFOSR Molecular Dynamics Conference, San Diego, CA

2009 SynCon, University of Southern California, Los Angeles, CA

Gillespie Symposium, Hamilton, ONT, Canada, 2009

European Materials Research Conference, Strasbourg, France, 2009

19th International Fluorine Symposium, Jackson Hole, WY, 2009

Inaugural Neil Bartlett Memorial Lecture, University of California, Berkeley, CA 2009

DTRA Program Review, Springfield, VA, 2009

Hermann Josef Frohn Lecture, University of Duisburg, Germany, 2010

DTRA Workshop, Eglin, FL, 2010

16th European Symposium on Fluorine Chemistry, Ljubljana, Slovenia, 2010

DTRA Program Review, Springfield, VA, 2010

Halchem V, Cagliari, Sardenia, 2010

Pacific Basin Countries Conference, Honolulu, HI, 2010

ACS Winter Fluorine Conference, St. Pete, FL, 2011

Workshop on Energetic Materials, University of Maryland, 2011

Molecular Dynamics Conference, Pasadena, CA, 2011

DTRA Program Review, Springfield, VA, 2011

ACS National Meeting, Denver, CO, 2011

ONR Peer Review, National Harbor, 2011

International Indian Fluorine Symposium, New Delhi, India, 2012

ACS National Meeting, San Diego, CA, 2012 (4 papers)

AFOSR Molecular Dynamics Conference, Arlington, VA, 2012

Pyrotechnics Workshop, Denver, CO, 2012

Arizona State University, Seminar, Tempe, AZ, 2012

Gordon Conference, Mount Snow, VT, 2012 (2 papers)

ONR/AFOSR Energetic Materials Review, Arlington, VA, 2012

International Fluorine Symposium, Kyoto, Japan, 2012

Seminar, FU Berlin, Germany, 2012

Seminar, Cal State University, Long Beach, CA, 2012

AFOSR/AFRL, Synthesis Conference, Pasadena, CA, 2012

Collaborations with other Groups

NAVAIR China Lake: Kelvin Higa and Curtis Johnson

NSWC Indian Head: Jim Lightstone and Jillian Horn

AFRL Edwards: Jerry Boatz, Stefan Schneider, Tommy Hawkins, Thorsten Schroer, Angelo Alfano

University of Alabama, Tuscaloosa: David Dixon

Oak Ridge National Laboratory: A. Kolesnikov

NIST: Liu

New Discoveries, Inventions, or Patent Disclosures

K. O. Christe and G. Drake, "Energetic Ionic Liquids," US Patent 7,771,549, Aug. 10, 2010.

K. Higa, K. O. Christe, R. Haiges. "High-Energy and High Density Compositions for the Defeat of Chemical and Biological Agents," US Patent Application.

Honors/Awards

K. O. Christe: Elected as a Fellow to the European Academy of Sciences, Liege, Belgium, (2009).

K. O. Christe: Inaugural Neil Bartlett Memorial Lecturer, University of California, Berkeley, (2009).

K. O. Christe: Elected as a Fellow to the European Academy of Sciences and Arts, Salzburg, Austria (2010).

K. O. Christe: ACS Tolman Award (2011).

R. Haiges: Robert Bau Award, University of Southern California (2011).

DEPARTMENT OF DEFENSE

DEFENSE TECHNICAL
INFORMATION CENTER
8725 JOHN J. KINGMAN ROAD,
SUITE 0944
FT. BELVOIR, VA 22060-6201
ATTN: DTIC/OCA

DEFENSE THREAT REDUCTION
AGENCY
8725 JOHN J. KINGMAN ROAD
STOP 6201
FT. BELVOIR, VA 22060-6201
ATTN: S. PEIRIS

DEPARTMENT OF DEFENSE
CONTRACTORS

EXELIS, INC.
1680 TEXAS STREET, SE
KIRTLAND AFB, NM 87117-5669
ATTN: DTRIAC